

Magnetic Reversal on Vicinal Surfaces

R.A. Hyman¹, A. Zangwill¹, and M.D. Stiles²

¹*School of Physics, Georgia Institute of Technology, Atlanta, GA 30332-0430*

²*Electron Physics Group, National Institute of Standards and Technology, Gaithersburg, MD*

20899

(February 10, 1999)

Abstract

We present a theoretical study of in-plane magnetization reversal for vicinal ultrathin films using a one-dimensional micromagnetic model with nearest-neighbor exchange, four-fold anisotropy at all sites, and two-fold anisotropy at step edges. A detailed “phase diagram” is presented that catalogs the possible shapes of hysteresis loops and reversal mechanisms as a function of step anisotropy strength and vicinal terrace length. The steps generically nucleate magnetization reversal and pin the motion of domain walls. No sharp transition separates the cases of reversal by coherent rotation and reversal by depinning of a 90° domain wall from the steps. Comparison to experiment is made when appropriate.

PACS numbers:75.70.Ak,75.60.-d,75.10.Hk

I. INTRODUCTION AND BACKGROUND

Laboratory studies of ultrathin films of transition metals confirm the general principle that broken symmetry induces magnetic anisotropy. [1,2] The most common example is the loss of translational invariance at the free surface of a film or at an internal interface of a multilayer structure. The phenomenological “broken-bond” model of Néel [3] then provides an intuitive way to understand why atoms at the surface or interface favor alignment of their magnetic moments either parallel or perpendicular to the broken symmetry plane. [4] In some cases, perpendicular anisotropy occurs that is strong enough to overwhelm the tendency for in-plane magnetization favored by magnetostatic shape anisotropy. This situation can be exploited for a variety of applications and has been the subject of very thorough experimental and theoretical work. [5]

In this paper, we focus on a related phenomenon: the magnetic anisotropy induced by crystallographic steps on the surface of a single crystal film. Here, it is the loss of translational invariance in directions parallel to the (nominal) surface plane that is germane. Application of the Néel model suggests that local moments will tend to align themselves either parallel or perpendicular to the local step orientation. The magnitude of the effect (on a per atom basis) is predicted to be comparable to conventional surface anisotropy. However, it was not until 1987 that Hillebrands *et al.* invoked step-induced anisotropy to rationalize their surface spin wave data for epitaxial Fe/W(110). [6] Since all ultrathin films invariably have step edges (associated either with steps on the substrate or with the nucleation and growth of monolayer height islands during the growth process) it is not surprising that subsequent experimental studies often cite this phenomenon in connection with “surface roughness effects”. [7]

We recently presented a theoretical study of in-plane magnetization reversal in ultrathin films with step structure in typical samples. [8] The model film was comprised of an array of square, monolayer-height, magnetic islands of variable size and density on top of a few complete magnetic layers. Classical XY-type spins at each site were presumed to rotate in

the surface plane subject to nearest-neighbor ferromagnetic exchange, an intrinsic four-fold in-plane anisotropy at all surface sites, Zeeman energy from an external field, and a two-fold anisotropy at island perimeter sites only. Numerical simulations and simple geometric scaling arguments predicted significant variations in coercivity as a function of coverage for layer-by-layer growth at low island nucleation densities. This result was found to be in semi-quantitative agreement with the surface magneto-optic Kerr effect (SMOKE) data of Buckley *et al.* [9] for the Cu/Co/Cu(001) system. A subsequent Monte Carlo simulation study [10] of coercivity in islanded Fe sesquilayers on W(110) using an in-plane Ising-type spin model yielded similarly good results in comparison to experiment.

The theoretical results of Ref. [8] were interpretable on the basis of several qualitative concepts: (i) nucleation of magnetization reversal at island edges; (ii) pinning of domain walls at island edges; and (iii) fusion of nearby domains. Unfortunately, even the simple island morphology studied there was still too complex to permit a detailed analytic treatment of the reversal process as one might desire. For this reason, we analyze an even simpler problem in this paper: zero-temperature, in-plane magnetization reversal in ultrathin vicinal films. The basic model sketched above remains unchanged except that the morphology is simplified to a periodic array of flat magnetic terraces separated by straight, monolayer-height steps. This renders the problem one-dimensional and amenable to analytic study.

One-dimensional models of magnetization reversal with inhomogeneous or competing anisotropies have been a fixture of the magnetism literature for many years. Most of these papers focus on the demonstration that planar defects in bulk ferromagnets can nucleate reversal and/or pin domain wall motion. If operative, these effects call into question the suitability of the popular single-domain, coherent rotation model of Stoner and Wohlfarth [11] as a description of magnetization reversal. Filipov [12] and later Brown [13] studied the effect of surface anisotropies on the nucleation field (where the magnetization first deviates from its saturation value) while Mitsek and Semyannikov [14] and later Friedberg and Paul [15] focused on the depinning of pre-existing reversed domains as a determinant of the coercive field (where the magnetization projected on the external field direction first falls to

zero). In recent years, Arrott has been explicit in the application of these ideas to ultrathin films with and without step structure. [16] Our analysis will be seen to substantially extend all of these studies.

On the experimental side, Heinrich *et al.* [17] first drew attention to the fact that a step-induced uniaxial anisotropy must be present on vicinal surfaces. Subsequent work confirmed this observation [18–20] and revealed a number of other systematic features. As particular motivation for the present work, we draw attention to the SMOKE data of Kawakami *et al.* [21] obtained from Fe films grown on stepped Ag(001) substrates. Characteristic “split-loop” hysteresis curves were found where the degree of splitting varied smoothly with the degree of vicinality. The authors interpreted their results using a single domain switching model where the step edge anisotropy was distributed over the entire surface. The analysis below will make clear the extent to which this description can be regarded as reliable.

The plan of our paper is as follows. Section II is an overview that includes (i) a discussion of the model assumptions; (ii) the definition of important dimensionless quantities and the presentation of a “phase diagram” that catalogs the possible hysteresis loop topologies that can occur; (iii) a qualitative discussion of the physical mechanisms of magnetization reversal that can occur; and (iv) a preliminary comparison to relevant experiments. Section III reports our mathematical procedures. We define the Hamiltonian used and solve the model exactly to extract the physics of zero-temperature reversal in the single domain and single step limits. The intermediate case of multiple steps is formulated and solved numerically. Section IV is a discussion that complements the earlier overview in light of our analytic and numerical results. We consider the crossover between coherent rotation and domain wall depinning, discuss relevant experiments in more detail, and comment on various limitations and extensions of the model. Section V summarizes our results and concludes the paper.

II. OVERVIEW

A. Model Assumptions

We consider a uniformly thick ultrathin magnetic film adsorbed onto a vicinal non-magnetic substrate. By flat, we mean that the film has no island structure, *e.g.* a film grown in step flow mode. [22] By ultrathin, we mean that there is no significant variation in the magnetization density in the direction perpendicular to the plane of the substrate terraces. By vicinal, we mean a sequence of flat terraces of length L separated by monoatomic height steps. We assume perfectly straight steps so that the spin configuration is a function only of the spatial coordinate perpendicular to the steps. The problem is thereby reduced to a one-dimensional classical spin chain with ferromagnetic exchange J .

The total surface anisotropy from all sources is presumed to compel the spins to lie in the plane of the substrate terraces. To model surfaces with cubic symmetry, we assign a four-fold anisotropy with strength K_4 to every site of the chain and a two-fold anisotropy with strength K_2 to every step site. The sign of K_4 is chosen to favor spin orientations parallel and perpendicular to the steps. [23] If the sign of K_2 favors spin orientation parallel (perpendicular) the steps, we apply the external field H perpendicular (parallel) to the steps. These cases are identical by symmetry. Magnetostatics contributes to the total surface anisotropy that compels the spins to lie in-plane. For this model, with in-plane spins, magnetostatics is not treated explicitly because its additional effects are known to be negligible in the ultrathin limit. [24] Figure 1 is a schematic representation of the physical situation and the spin chain model studied here.

For simplicity, we choose units where the lattice constant a is one and J , K_4 , K_2 , and H , all have units of energy. To recover dimensional units as used in [8], divide K_4 and K_2 by a^2 , and divide H by μ , where μ is the atomic magnetic moment.

B. The Phase Diagram

We organize our discussion of hysteresis in this system around a “phase” diagram (Figure 2) whose axes are a scaled step anisotropy strength $\mathcal{K} = K_2/2\sigma$ and a scaled terrace length $\mathcal{L} = L/W$ where K_2 is the step anisotropy energy, $\sigma = \sqrt{2JK_4}$ is the domain wall energy, and $W = \sqrt{J/2K_4}$ is the exchange length. The solid lines delineate four distinct hysteresis loop topologies. The dashed lines divide Phase II into three sub-variants.

Figure 3 illustrates representative hysteresis loops in each phase. Since all the loops are symmetric with respect to the sign of H , it will be convenient to restrict discussion to the situation where the field changes from positive to negative. We define three characteristic values of the external field. The first deviation of the magnetization from saturation occurs at the nucleation field H_N . A jump in magnetization that initiates at the steps is denoted H_S . A magnetization jump that initiates on the terraces is denoted $-H_T$. $H_S = H_N$ in Phases IIc, III & IV.

In phase I, all spins rotate continuously from the saturation direction to the reversed direction as the external magnetic field is reversed adiabatically. Near the left hand side of the phase diagram, the spins rotate nearly coherently as a single unit. This is called Stoner-Wohlfarth behavior. [11] But near the right hand boundary of the Phase I field, the spins near the step edge rotate more (per unit change in external field) than do the spins near the center of the terrace. There is no hysteresis, *i.e.*, no jumps appear in the magnetization curve, merely more or less spatially inhomogeneous spin rotation.

In Phase IIa, spins within an exchange length of a step rotate away from the saturation direction at H_N in response to the torque applied by the step anisotropy. A domain wall thus forms between the step spins and the remaining terrace spins. A field-dependent energy barrier Δ_{DW} separates this configuration from a configuration where all spins point nearly 90° from the saturation direction. $\Delta_{DW} \rightarrow 0$ at H_S and the domain walls “depin” from the steps and sweep across the terraces. The accompanying jump in magnetization is followed by a continuous segment of the hysteresis curve that passes through the origin. This is an

SW-like regime of nearly coherent spin rotation. During this rotation, an energy barrier Δ_{SW} separates the terrace spin configuration from the nearly reversed state. At $H = -H_{\text{T}}$, Δ_{SW} disappears for the terrace spins farthest from the steps and a second jump in magnetization occurs. Reversal completes at $-H_{\text{N}}$ when the step spins finally complete their rotation.

Phase IIb differs from Phase IIa because $H_{\text{T}} > H_{\text{N}}$ and the final jump in magnetization carries the system directly to the saturated reversed state. The phase boundary is the locus of points where $H_{\text{T}} = H_{\text{N}}$. Note that there is a small range of \mathcal{K} where one encounters the phase sequence IIa \rightarrow IIb \rightarrow IIa as \mathcal{L} decreases from large values.

Phase IIc mostly occupies a portion of the phase diagram where $\mathcal{K}\mathcal{L} < 1$. In this regime, the independent domain wall description used above is no longer appropriate because the walls have overlapped to the point where the magnetization inhomogeneity across each terrace is not large. The reversal is better described as nearly coherent rotation, as above, where the degree of rotation differs for spins near and far from the steps. On the other hand, a thin sliver of the IIc phase field extends to very large values of \mathcal{L} where the independent domain wall picture remains valid. This shows that there is no rigid correspondence between phases and reversal mechanisms. More typically, as in this case, there is a smooth crossover from a domain wall picture to a coherent rotation picture.

Phase III occupies the smallest portion of the phase diagram. The step anisotropy here is sufficiently small that a negative field is needed to nucleate reversal. Otherwise, the reversal mechanism is identical to Phase IIc.

Phase IV is characterized by $H_{\text{N}} < -H_{\text{T}}$ so that only a single magnetization jump occurs. In fact, H_{N} is so negative that the state with terrace spins nearly parallel to the step is not stable as it was in Phase III. During the jump, the degree of spatial homogeneity of the spin rotation is dictated by the magnitude of $\mathcal{K}\mathcal{L}$. Nearly coherent SW reversal occurs when $\mathcal{K}\mathcal{L} \ll 1$ while rotation initiates at the step when $\mathcal{K}\mathcal{L} \gg 1$.

C. Relevant Experiments

Two recent experimental studies of magnetization reversal in thin iron films deposited onto vicinal and (nominally) flat surfaces can be interpreted with our phase diagram. Chen and Erskine [19] studied ultrathin Fe/W(001) where the step anisotropy favors magnetic moment alignment perpendicular to the step. Their results for an external magnetic field aligned parallel to the steps can be compared with our results by symmetry. They observe loops characteristic of Phase III and Phase II for the samples they label “smooth” and “stepped” for 1.5 ML iron coverage.

Kawakami et al. [21] presented a sequence of four hysteresis loops for the Fe/Ag(001) system that we interpret similarly as a transition from Phase III to Phase II. In this case, the step anisotropy favors magnetic moment alignment parallel to the step and the data they present for the external field aligned perpendicular to the step is relevant. More details of this comparison can be found in the Discussion section.

III. QUANTITATIVE ANALYSIS

A. General Results

In the continuum limit, the model assumptions stated at the beginning of section II lead us to the following expression for the magnetic energy per unit length of step for an ultrathin film on a vicinal surface:

$$E = \int dx \left[\frac{1}{2} J \left(\frac{d\theta}{dx} \right)^2 - \frac{1}{2} K_4 \cos 4\theta - H \cos \theta + \frac{1}{2} K_2 \sum_S \delta(x - x_S) \cos 2\theta \right]. \quad (1)$$

We remind the reader that J , K_4 , K_2 , and H all have units of energy. The lattice constant is unity so the integration variable x is dimensionless. The function $\theta(x)$ is the angular deviation of the magnetization density from the field direction at point x . For definiteness, we take the latter to be perpendicular to the steps and pointing down the vicinal staircase

of Figure 1. Note that the two-fold anisotropy acts only on step edge spins at the discrete positions x_S .

We seek spin configurations $\theta(x)$ that correspond to local minima of (1). In general, an energy minimum moves smoothly in configuration space as H changes and the corresponding spin configuration and magnetization change smoothly as well. Apart from accidental degeneracies, the only exception to this behavior occurs when the energy minimum evolves to a saddle point. At that point, the spin configuration changes discontinuously, a new energy minimum is adopted, and a jump appears in the magnetization curve. Our goal is to calculate the field values where these jumps occur. Their number and sign distinguish the phases of the system.

The Euler-Lagrange equation that determines the extremal configurations of (1) is [25]

$$J \frac{d^2\theta}{dx^2} = H \sin \theta + 2K_4 \sin 4\theta - \sum_S \delta(x - x_S) K_2 \sin 2\theta. \quad (2)$$

We seek solutions of this equation with the same periodicity as the steps. These solutions are parameterized by two constants, the spin angle at the center of each terrace θ_T and the spin angle at each step θ_S . One equation that relates these two is obtained as follows. Place the origin $x = 0$ at a step, multiply (2) by $d\theta/dx$, and integrate from the center of the terrace ($x = -L/2$) to an arbitrary point x on the same terrace. The result is

$$H \cos \theta_T + \frac{1}{2} K_4 \cos 4\theta_T = \frac{1}{2} J \left(\frac{d\theta}{dx} \right)^2 + H \cos \theta + \frac{1}{2} K_4 \cos 4\theta \quad (3)$$

using the fact that $d\theta/dx = 0$ at the center of the terrace.

The constant θ_S appears when we evaluate (3) at a step. For this purpose, integrate (2) from $x = 0^-$ to $x = 0^+$ and use reflection symmetry across the step, i.e.,

$$\left. \frac{d\theta}{dx} \right|_{0^+} = - \left. \frac{d\theta}{dx} \right|_{0^-}, \quad (4)$$

to get

$$2J \left. \frac{d\theta}{dx} \right|_{0^-} = K_2 \sin 2\theta_S. \quad (5)$$

Substitution into (3) yields

$$\begin{aligned} \mathcal{K}^2 \sin^2 2\theta_S = \mathcal{H}(\cos \theta_T - \cos \theta_S) \\ + (\cos 4\theta_T - \cos 4\theta_S)/2 \end{aligned} \quad (6)$$

which relates θ_T and θ_S as desired. The scaled magnetic field $\mathcal{H} = H/K_4$.

A second relation between θ_T and θ_S can be found that involves the terrace length explicitly by integrating (3) from the center of a terrace to the step edge:

$$\mathcal{L} = 2 \int_{\theta_T}^{\theta_S} \frac{d\theta}{\sqrt{[\mathcal{H}(\cos \theta_T - \cos \theta) + (\cos 4\theta_T - \cos 4\theta)/2]}} \quad (7)$$

The analysis to this point is completely general and forms the basis for all the approximate analytic and numerical results that follow. We begin our discussion with two special situations that can be treated in full analytically: the single domain limit and the single step limit.

B. The Single Domain limit

This section focuses on the bottom left corner of the phase diagram where $\mathcal{L}\mathcal{K} \ll 1$. This is the Stoner-Wohlfarth limit where only a single homogeneous magnetic domain is present. The energy per terrace per unit length of step $\tilde{E} = E/L$ is

$$\tilde{E} = -\frac{1}{2}K_4 \cos 4\theta + \frac{1}{2}\tilde{K}_2 \cos 2\theta - H \cos \theta, \quad (8)$$

where the value of the effective two-fold anisotropy $\tilde{K}_2 = K_2/L$, as can be verified by substitution of a uniform spin configuration $\theta(x) = \theta$ into (1).

In terms of the magnetization $M = \cos \theta$, we seek the stationary points of the quartic expression

$$\tilde{E} = -K_4(2M^2 - 1)^2 + \tilde{K}_2 M^2 - HM, \quad (9)$$

i.e, the solutions of

$$\frac{d\tilde{E}}{d\theta} = \sin\theta [H - \tilde{H}(M)] = 0. \quad (10)$$

where

$$\tilde{H}(M) = (2\tilde{K}_2 + 8K_4)M - 16K_4M^3. \quad (11)$$

The extremal condition is satisfied trivially when the magnetization is parallel or antiparallel to the field direction where $\sin\theta = 0$. But it is also satisfied by the cubic equation $H = \tilde{H}(M)$. In either case, we must have

$$\frac{d^2\tilde{E}}{d\theta^2} = \cos\theta [H - \tilde{H}(M)] + \sin^2\theta \frac{d\tilde{H}(M)}{dM} > 0 \quad (12)$$

to guarantee that the solution is a local minimum of the energy.

The first term on the right hand side of (12) determines the extremal properties of the $\sin\theta = 0$ solutions. The $\theta = 0$ solution is a local minimum for $H > H_N^0$ where

$$H_N^0 = H_S^0 = 2\tilde{K}_2 - 8K_4 \quad (13)$$

is the limiting value of the nucleation field when $\mathcal{L}\mathcal{K} \ll 1$. Notice that portions of Phases I, IIc, III, and IV appear in this limit where the nucleation field H_N^0 and the first jump field H_S^0 are coincident. The $\theta = \pi$ solution is a local minimum for $H < -H_N^0$. At finite temperature, spin configurations at local minima of the free energy become metastable since thermal fluctuations can excite the system over energy barriers to a lower energy minimum. These fluctuations decrease the area of hysteresis loops. [26]. For example, as the nucleation field is approached from above, the energy barrier to the unsaturated state goes to zero as

$$\Delta\tilde{E} = (H - H_N^0)^2 \left(-2 \frac{d^2\tilde{E}}{dM_N^2} \right)^{-1} \frac{1}{(H - H_N^0)^2 (80K_4 - 4\tilde{K}_2)^{-1}} \quad (14)$$

where $d^2\tilde{E}/dM_N^2$ is evaluated at the saturation magnetization $M_N = 1$. At finite temperatures a hysteretic jump can occur due to thermal fluctuations when ΔE is of the order $k_B T$. Therefore H_N^0 is a lower bound for the jump field. The actual jump field will be larger than this by an amount

$$\Delta H_{\text{N}}^0 \propto \sqrt{(80K_4 - 4K_2)k_{\text{B}}T}. \quad (15)$$

The second term on the right hand side of (12) determines the extremal properties of the $H = \tilde{H}(M)$ solutions. Because the coefficient of the cubic term is negative, at most one of the three solutions to the cubic equation satisfies $d\tilde{H}(M)/dM > 0$. This means that the magnetization increases (decreases) when the field increases (decreases)—a condition that is met when $|H| < |H_{\text{T}}^0|$ where

$$H_{\text{T}}^0 = \frac{8\sqrt{6}}{9}K_4\left(1 + \frac{\tilde{K}_2}{4K_4}\right)^{5/2} \quad (16)$$

is the limiting value of the jump field when $\mathcal{L}\mathcal{K} \ll 1$. This is true unless $\tilde{K}_2 > 20K_4$ in which case the $H = \tilde{H}$ solution is stable for all values of M and there are no magnetization jumps for any value of external field. When $\tilde{K}_2 + 8K_4 < 0$, the $H = \tilde{H}(M)$ solution is never stable and the $\sin \theta = 0$ solutions are the only local minima. As the jump field is approached from below, the energy barrier to the saturated state goes to zero as

$$\begin{aligned} \Delta \tilde{E} &= \frac{2}{3}(H_{\text{T}}^0 - H)^{3/2} \left(-\frac{1}{8} \frac{d^3 \tilde{E}}{dM_{\text{T}}^3} \right)^{-1/2} \\ &= \frac{2}{3}(H_{\text{T}}^0 - H)^{3/2} \left(3K_4(2\tilde{K}_2 + 8K_4) \right)^{-1/4} \end{aligned} \quad (17)$$

where $d^3 \tilde{E}/dM_{\text{T}}^3$ is evaluated at

$$M_{\text{T}} = \sqrt{(2\tilde{K}_2 + 8K_4)/48K_4}, \quad (18)$$

the zero temperature magnetization at $H = H_{\text{T}}^0$. At finite temperature the jump field is smaller than H_{T}^0 by an amount

$$\Delta H_{\text{T}}^0 \propto \left(\left(\frac{3}{2}k_{\text{B}}T \right)^2 \sqrt{3K_4(2K_2 + 8K_4)} \right)^{1/3}. \quad (19)$$

Away from the single domain limit the qualitative effects of finite temperature are the same but are more difficult to treat analytically.

The above results can be applied to find analytic formulae for the three phase boundaries in the lower left corner of the phase diagram. The system is in phase I when $\tilde{K}_2 > 20K_4$

since, as noted, the magnetization curve has no jumps. The remanent slope is $dM/dH = 1/(2\tilde{K}_2 + 8K_4)$. For $20K_4 > \tilde{K}_2 > 4K_4$, the system is in phase IIc. The remanent slope is $dM/dH = 1/(2\tilde{K}_2 + 8K_4)$. For $4K_4 > \tilde{K}_2 > 2K_4$ the system is in phase III. Phase IV occurs when $2K_4 > \tilde{K}_2$. Using these results and $\tilde{K}_2 = K_2/L$, the boundaries between the phases near the origin are: $\mathcal{K} = 5\mathcal{L}$ between phases I and IIc, $\mathcal{K} = \mathcal{L}$ between phases IIc and III, and $\mathcal{K} = \frac{1}{2}\mathcal{L}$ between phases III and IV.

C. The Single Step limit

The right edge of the phase diagram where $\mathcal{L} \rightarrow \infty$ is the limit where the step separation is large compared to the exchange length and the (somewhat larger) domain wall width. In that case, it is sufficient to study the case of a single step bounded by semi-infinite terraces on each side. Our goal again is to calculate the nucleation field H_N and the jump fields H_S and H_T . We do this by focusing attention on the spin at the step where $\theta = \theta_S$ and the spins at $\pm\infty$ where we assume that θ approaches the constant value θ_T .

The fact that $\theta(x) \rightarrow \theta_T$ as $x \rightarrow \pm\infty$ implies that all spatial derivatives of $\theta(x)$ vanish at infinity. Applying this to (2) yields

$$H \sin \theta_T + 2K_4 \sin 4\theta_T = 0 \quad (20)$$

which determines θ_T . To find θ_S , we need only note that the $\theta_T = 0$ solution to (20) is valid for large values of the external field. We therefore substitute this value into (6) to find

$$\frac{1}{2}(\mathcal{K}^2 - 1) \sin^2 2\theta_S = \mathcal{H} \sin^2 \frac{1}{2}\theta_S. \quad (21)$$

The identification

$$H_N^\infty = 8K_4(\mathcal{K}^2 - 1). \quad (22)$$

follows immediately since, by definition, θ_S is very small near nucleation. Substitution of (22) into (21) gives

$$H = H_N^\infty \cos^2 \theta_S \cos^2 \frac{1}{2} \theta_S \quad (23)$$

which is valid so long as $\theta_T = 0$ and $H < |H_N^\infty|$.

The case $H_N^\infty > 0$ is relevant to Phases IIa and IIb where H_S^∞ is distinct from H_N^∞ . In particular, the step angle θ_S increases smoothly as H decreases until the latter reaches

$$H_S^\infty = 0 \quad (24)$$

when a magnetization jump occurs because (23) has no solutions for $H < 0$. The spin configuration just before the jump is precisely that of a 90° domain wall because $\theta_S = \pi/2$ and $\theta_T = 0$. As noted in Section II, the jump occurs because the domain wall depins from the step and sweeps across the terrace so that final state has $\theta(x) = \pi/2$ and $M = 0$. An explicit formula for H_T^∞ can be found by noting that this jump initiates with the terraces spins at $\pm\infty$. These obey the pure Stoner-Wohlfarth dynamics of Section II.B with $\tilde{K}_2 = 0$. In particular, (20) is identical to (10). The final magnetization jump thus occurs at $-H_T^\infty$ where

$$H_T^\infty = \frac{8\sqrt{6}}{9} K_4. \quad (25)$$

This value is a lower bound for the jump field when the terrace length is finite because the presence of nearby steps retards the final transition to the reversed state.

The case $H_N^\infty < 0$ applies to Phases III and IV. The above discussion shows that at nucleation in Phase III, the saturated state jumps immediately to the spin configuration that satisfies (20) with $\theta_T \neq 0$. This state evolves smoothly until the magnetization jump at $-H_T^\infty$. In Phase IV, there is only a single jump because now (20) has stable solutions only at $\theta = 0$ and $\theta = \pi$ when $H = H_N^\infty$.

The boundaries between the various phases in the limit $\mathcal{L} \rightarrow \infty$ can be found quite simply. The IIa-IIb boundary is the locus of points where $H_T = H_N$. From (22) and (25) we get $\mathcal{K} = (1 + \frac{\sqrt{6}}{9})^{1/2} \approx 1.13$. The IIb-III boundary occurs when $H_N = 0$, i.e., $\mathcal{K} = 1$. The III-IV phase boundary is the locus of points where $H_N = -H_T$. This gives $\mathcal{K} = (1 - \frac{\sqrt{6}}{9})^{1/2} \approx 0.85$.

D. Other Analytic Results

This section presents three analytic results that pertain to interior portions of the phase diagram. The first is an implicit expression for the nucleation field at any point in the phase diagram. The second is an exact expression for the entire boundary between Phase IIc and Phase III. The third is the leading correction to the Phase II jump field H_S^∞ when the terrace length is finite.

For the nucleation field, our interest is the first deviation of the spin configuration from $\theta(x) \equiv 0$. We thus expand (2) to first order in θ :

$$J \frac{d^2 \theta}{dx^2} = (H + 8K_4)\theta - \delta(x)2K_2\theta. \quad (26)$$

Without the delta function, the appropriate solution to (26) is

$$\theta = A \cosh(\sqrt{(H + 8K_4)/J}x) \quad (27)$$

where A is a constant. Similarly linearizing the boundary condition (5) gives

$$2J \frac{d\theta}{dx} \Big|_{L/2} = -2J \frac{d\theta}{dx} \Big|_{-L/2} = 2K_2\theta_S. \quad (28)$$

Combining these results yields the implicit formula

$$-2K_2 + 2\sqrt{J(H_N + 8K_4)} \tanh \left[\frac{L}{2} \sqrt{\frac{H_N + 8K_4}{J}} \right] = 0. \quad (29)$$

for the nucleation field H_N . We obtain a more compact form by defining a shifted and scaled nucleation field \tilde{H}_N from

$$H_N(K_2, K_4, J, L) = -8K_4 + 8K_4 \tilde{H}_N(\mathcal{K}, \mathcal{L}). \quad (30)$$

and substituting (30) into (29). The final result

$$\mathcal{K} = \tilde{H}_N^{1/2} \tanh \left(\mathcal{L} \tilde{H}_N^{1/2} \right). \quad (31)$$

gives the nucleation field at any point in the phase diagram. Note the limiting forms $\tilde{H}_N = \mathcal{K}/\mathcal{L}$ for $\mathcal{K}\mathcal{L} \rightarrow 0$ and $\tilde{H}_N = \mathcal{K}^2$ for $\mathcal{K}\mathcal{L} \rightarrow \infty$. These are the Stoner-Wohlfarth and single

step results obtained earlier. The line $\mathcal{K}\mathcal{L} = 1$ can be regarded as a crossover between the two. We return to this point in Section IV.

The IIc-III phase boundary is defined by $H_N = 0$, i.e., $\tilde{H}_N = 1$. Substitution of this into (31) gives

$$\mathcal{K} = \tanh(\mathcal{L}) \tag{32}$$

which is the equation of the phase boundary drawn in Figure 2.

We turn finally to a calculation of the jump field H_S in Phase II for large but finite terrace lengths. In this limit, the domain wall depinning picture of the jump is appropriate. The calculation is analogous to the computation in Section III.C except that the single step formula (20) is replaced by a more general relation between θ_S and θ_T obtained from a variational form for the spin configuration near H_S .

Just below (24), we observed that the single-step spin configuration $\theta(x)$ just before the magnetization jump at H_S^∞ takes the form of a 90° domain wall. That is,

$$\tan \theta = e^{\pm \lambda x} \tag{33}$$

where $\lambda = \sqrt{8K_4/J}$. Since $\theta_S \simeq \pi/2$ at every step, an appropriate trial function for a multi-step system is obtained by adding together the \pm wall configurations from (33) in the form

$$\tan \theta = \tan \theta_T \cosh \lambda x, \tag{34}$$

which becomes

$$\tan \theta_S = \tan \theta_T \cosh \mathcal{L} \tag{35}$$

at each step. Expanding (35) for large \mathcal{L} and small $\epsilon = \pi/2 - \theta_S$ and θ_T gives

$$\epsilon = \frac{1}{2\theta_T} e^{-\mathcal{L}}. \tag{36}$$

Performing a similar expansion on (6) and retaining terms to lowest order in H only yields

$$H = \frac{2}{\theta_T^2} H_N^\infty e^{-2\mathcal{L}} + 4K_4\theta_T^2 \quad (37)$$

when (36) is used. The jump field

$$H_S = 2\sqrt{8K_4H_N^\infty} e^{-\mathcal{L}} \quad (38)$$

is the smallest value of H for which solutions to (37) exist for some value of θ_T .

E. Numerical Results

Numerical methods were used to study three aspects of this problem: (i) calculation of the hysteresis loops; (ii) determination of the \mathcal{L} dependence of the jump fields for representative values of \mathcal{K} ; and (iii) determination of the phase boundaries in the phase diagram.

The hysteresis loops in Figure 3 were computed directly from (1). For each choice of control parameters, the evolution of the stable energy minimum was followed by a combination of conjugate gradient (CG) minimization and spin relaxation dynamics. The initial state was chosen as the saturated state and the external field was reversed in small steps from a large positive value to a large negative value. The CG method reliably follows the adiabatic minimum until a magnetization jump occurs. But when a jump connects local energy minima that are far separated in configuration space, the CG scheme often predicts an obviously incorrect final state. To correct this, CG was used consistently except in the immediate vicinity of a jump. When it predicted a jump, the simulation was backed up and spin relaxation dynamics used to find the correct final state.

The nucleation field is found readily numerically from the general formula (29). A more elaborate procedure is needed to find the jump fields. Jumps in magnetization correspond to discontinuous changes in the spin configuration. In particular, $\partial\theta_T/\partial H$ diverges at both H_S and H_T . But since \mathcal{L} is a constant for a given physical situation, it must be the case that

$$\frac{d\mathcal{L}}{dH} = \frac{\partial\mathcal{L}}{\partial H} + \frac{\partial\mathcal{L}}{\partial\theta_T} \frac{\partial\theta_T}{\partial H} = 0. \quad (39)$$

In this equation, \mathcal{L} is regarded as a function of θ_T and H only since θ_S is a function of θ_T and H from (6). We conclude that there is a one-to-one correspondence between the divergences of $\partial\theta_T/\partial H$ and the zeros of $\partial\mathcal{L}/\partial\theta_T$.

The argument above directs us to find $\mathcal{L}(\theta_T)$ for any desired choice of \mathcal{K} and \mathcal{H} . Once this choice is made, we sample many values of θ_T in the interval $0 \leq \theta_T \leq \pi/2$. For each θ_T , we solve (6) for θ_S and integrate (7) to get \mathcal{L} . Figure 4 shows $\mathcal{L}(\theta_T)$ for $\mathcal{K}=1.25$ and $\mathcal{H}=2, 3, 4, 6, 9$. The value of \mathcal{H} decreases monotonically as the sequence of curves is traversed from bottom to top. All the curves approach either $\mathcal{L} = \infty$ as $\theta_T \rightarrow 0$ or possess a semi-infinite vertical segment at $\theta_T = 0$ that begins at the point where the curve hits the left \mathcal{L} axis.

We now argue that the horizontal dashed line labeled \mathcal{L}_S that is tangent to the local minimum of one of the displayed curves defines the physical terrace width for which the corresponding value of H is exactly H_S . H_S is encountered by reducing the field from large positive values where the spin configuration is saturated. The intersection of the line \mathcal{L}_S with the vertical portion of the curves for large \mathcal{H} confirms that $\theta_T = 0$ at saturation. As \mathcal{H} decreases, the corresponding curves eventually intersect the line \mathcal{L}_S at small non-zero values of θ_T . Finally, the intersection occurs at the local minimum of one of the curves. This is the curve of H_S because any further reduction in field leads to a discontinuous change in θ_T to the only remaining intersection point on the rightmost segment of the $\mathcal{L}(\theta_T)$ curves.

The horizontal dashed line labeled \mathcal{L}_T that is tangent to the local maximum of one of the curves defines the physical terrace width for which the corresponding value of H is exactly H_T . But since Fig. 4 is drawn for $H > 0$ only, the jump at H_T is encountered by increasing the external field from $H = 0$ where $M = 0$ [27]. The intersection of the line \mathcal{L}_T with the lowest field curve shown confirms that $\theta_T \simeq \pi/2$. As \mathcal{H} increases, the curves develop a local maximum and the intersection eventually occurs at this point. This is the curve of H_T because any further increase in field leads to a discontinuous change in θ_T to the only remaining intersection point on the leftmost segment of the $\mathcal{L}(\theta_T)$ curves.

The evolution of the nucleation and jumps fields as a function of \mathcal{L} found as described

above is illustrated in Figure 5 for $\mathcal{K} = 1.25$. Figure 6(a) confirms the exponential dependence of H_S on \mathcal{L} predicted in (38). Figure 6(b) shows that $H_T \sim \mathcal{L}^\chi$ for the last decade of data shown where $\chi \simeq 3.7$.

The relative values of H_N , H_T , H_S were used to construct all the phase boundaries shown in Figure 2. Figure 5 is germane to the I-IIa phase boundary. No jump fields exist for $\mathcal{L} < \mathcal{L}^*$ and $H_N > H_T > H_S$ for $\mathcal{L} > \mathcal{L}^*$. This is the same terrace length shown in Figure 4 where the dashed line $\mathcal{L} = \mathcal{L}^*$ intersects the curve of $\mathcal{L}(\theta_T)$ for which the extrema (and hence the jump fields) first disappear. The I-IIa phase boundary is asymptotically vertical as $\mathcal{K} \rightarrow \infty$. The limiting value of \mathcal{L}_∞^* is found from the same procedure as above by putting $\theta_S = \pi/2$ in (7). The result is $\mathcal{L}_\infty^* \approx 2.2072$.

Figure 7 shows the \mathcal{L} dependence of the nucleation and jump fields for $\mathcal{K} = 0.5$. The absence of the jump fields defines the range of Phase I as before. The other phases exhibit the relative orderings of the characteristic fields discussed in Section II, i.e., $H_N = 0$ defines the IIc-III boundary and $H_T = -H_N$ defines the III-IV boundary. Figure 8 shows the nucleation and jump fields for $\mathcal{K} = 1.17$. The re-entrant behavior IIa \rightarrow IIb \rightarrow IIa described in Section II arises because the curves of H_T and H_N intersect twice. The transition from IIa to IIb at fixed \mathcal{L} is readily understood. H_T is nearly independent of \mathcal{K} because it is related to terrace spin behavior far from the steps. But H_N decreases rapidly as \mathcal{K} decreases because the torque on step spins is reduced. Eventually, H_N drops below H_T for all values of \mathcal{L} . We omit a figure that shows the IIc-IIb phase boundary ($H_S = H_N$) explicitly.

We note finally that there is a critical point in the phase diagram $(\mathcal{K}_C, \mathcal{L}_C)$ where H_T , H_S , and H_N are coincident. This is the point in Figure 2 where the I-IIa, IIa-IIb, IIb-IIc, and IIc-I phase boundaries all meet. Our best estimate is $\mathcal{K}_C \approx 1.10$ and $\mathcal{L}_C \approx 0.56$.

IV. DISCUSSION

A. The Reversal Mechanism

An important conclusion from our analysis is that a distinct hysteresis loop topology does not imply a distinct mechanism of magnetization reversal. This is immediately clear from Figure 2 where all four phases are present in the $\mathcal{L}\mathcal{K} \ll 1$ limit of nearly coherent rotation and three of the four phases are present in the limit of widely separated steps where reversal occurs by domain wall depinning. No sharp transition separates these cases. Instead the reversal mechanism smoothly crosses over from coherent rotation to domain wall depinning as the terrace length or step anisotropy is increased.

The crossover is most easily understood for the case of nucleation which, as noted, always occurs at the steps due to the torque exerted on the saturated state by the local two-fold anisotropy. When $\mathcal{L}\mathcal{K} \gg 1$, nucleation results in the formation of a domain of rotated spins around each step separated from the unrotated terrace spins by a domain wall. Now suppose that \mathcal{L} is reduced, say, by increasing the vicinality of the substrate. The spins on the terrace rotate away from saturation when the domain walls begin to overlap. In the limit when $\mathcal{L} \ll \mathcal{K}^{-1}$, their rotation becomes indistinguishable from the rotation of the step spins and the coherent rotation picture is a good approximation to nucleation. Alternately, suppose that \mathcal{K} is reduced, say, by increasing the film thickness or by adsorbing foreign gases onto the steps. This reduces the torque on the step spins so that their angular deviation from the terrace spins is not as great. In the limit when $\mathcal{K} \ll \mathcal{L}^{-1}$, this difference nearly disappears and the coherent rotation picture is again appropriate.

We turn next to the first jump field H_S . Coburn and co-workers [28] have presented a model of reversal for ultrathin magnetic films with in-plane magnetization and four-fold anisotropy. They assume that the film is well described by a single homogeneous domain before and after every jump in the hysteresis curve. Domain walls are presumed to nucleate at widely separated surface steps or other defects. Magnetization jumps occur when the energy density

gain to make the transition ΔE is equal to a phenomenological energy density ϵ needed to depin the wall from the most effective pin in the film.

This description approximately reproduces our results when \mathcal{L} is large if we take account of the inhomogeneous spin configuration induced by the steps. In Section II, H_S was defined as the field when the energy barrier Δ_{DW} vanished. Here, $\Delta_{\text{DW}} = \epsilon - \Delta E$ where

$$\Delta E \simeq -H/a + 2\sigma/L + (A/L)e^{-\mathcal{L}} \quad (40)$$

and A is a constant with dimensions of energy. The first term is the Zeeman energy gain of the saturated state compared to the 90° state. The second term is the energy cost of the domain walls near the two steps that bound a terrace. The last term represents an effective repulsive interaction between neighboring walls that arises from the overlap of domain walls. The terrace spins in the overlap region pay anisotropy energy, and the energy of the initial state rises compared to the single step case. The exponential dependence on wall separation is familiar from other problems where periodic domains form, e.g, the commensurate-incommensurate transition. [29]

The condition $\Delta_{\text{DW}} = 0$ yields the estimate

$$H_S \simeq 2\sigma/L - \epsilon + (A/L)e^{-\mathcal{L}}. \quad (41)$$

This agrees with (38) up to the prefactor of the exponential if $\epsilon = 2\sigma/L$. This is not unreasonable because the barrier for the two domain walls to depin, sweep across their common terrace, and annihilate is associated with a spin configuration where the two walls are separated by a distance small compared to \mathcal{L} but large compared to the exchange length W . Of course, ϵ is not distributed across the terrace in any physical sense. It is associated solely with the particular spin configuration described just above.

B. Comparison to Experiment

We remarked in Section II.C that the shape of the SMOKE loops obtained by Chen and Erskine [19] for flat and vicinal ultrathin Fe/W(001) appear (to the eye) to be very similar

to our Phase III and phase II topologies, respectively. To see that this is not unreasonable, we combine the 25Å terrace widths reported in Ref. [19] with typical values of the magnetic parameters $J \sim 10^{-21}$ J, $K_2 \sim 1$ mJ/m², and $K_4 \sim 10^{-2}$ mJ/m² [2] to discover that this experiment corresponds to $\mathcal{L} \sim 1$ and $\mathcal{K} \sim 1$. This is indeed in the vicinity of the II-III phase boundary.

We assigned the same transition to the data of Kawakami *et al.* [21] for 25 ML of Fe on a sequence of surfaces vicinal to Ag(001). This is still nominally an ultrathin film because the exchange length $W = \sqrt{J/2K_4} \sim 20$ ML using the values above. In fact, the results of this experiment lay even closer to the lower left corner of our phase diagram than the Chen and Erskine experiment because the vicinality is greater.

The authors of Ref. [21] analyzed their data with a single domain model similar to that of Coburn and co-workers [28] except that the step anisotropy was distributed across the terraces and the depinning energy ϵ was set to zero. Such a model actually yields no hysteresis at all—just a magnetization curve with two symmetrical jumps. Magnetic parameters were extracted from the experiment by matching this jump to the average of what we call H_S and H_T . In our opinion, formulae similar to our (13) and (16) for H_S^0 and H_T^0 should be used to analyze the large vicinality data [30] of Ref. [21].

C. Extensions of the Model

It is easy to think of extensions of the model studied here that would render the results more directly comparable to experiment. Probably the most stringent assumption we make is that the magnetic film smoothly coats the vicinal substrate. For relatively small terrace lengths, this is possible if the deposition is performed at high temperature so that nucleation of islands on the terraces is suppressed and growth occurs in so-called “step-flow” mode. [22] Otherwise, it is necessary to take account of the effect of these islands on the hysteresis. This was the subject of a previous paper by us [8] for a square island geometry and we can use those results to suggest the effect in the present case.

For fixed deposition conditions, island nucleation is increasingly probable as the terrace length increases. [22] For this reason, we focus on the right hand side of the phase diagram. The magnetization jump at H_S will be interrupted because the domain walls depinned from the vicinal steps will not sweep completely across the terraces. Instead, they will be repinned by the channels between islands. This introduces additional jump structure into the hysteresis curves and likely will alter the coercive field significantly. We expect little change in H_T but there will be an extra magnetization jump before final reversal associated with spins that remain pinned in the original saturation direction at island edges perpendicular to the vicinal step edges.

The one-dimensional character of our model arises because we assumed perfectly straight steps. This is not generally the case because the desired step-flow growth mode itself induces a step-wandering instability. [31] This instability will have the effect of introducing two-fold anisotropies in a variety of directions and a random anisotropy model (with spatially correlated randomness) might be a suitable starting point in the limit of large waviness.

Non-uniform terrace widths are another feature of real vicinal surfaces that might also be treated in a more complete model. The result is easy to guess in the pinned limit where every terrace acts independently. Otherwise, nucleation and subsequent jumps will occur first in regions of the film with largest step density and eventually spread to regions of low step density.

Except for the single domain limit, where energy barriers can be calculated exactly, we have ignored thermal fluctuations. At low temperatures thermal fluctuation decrease the area of hysteresis loops. At higher temperatures fluctuations can qualitatively change loop structure and Monte Carlo methods become appropriate. [26].

Finally, we have ignored both perpendicular variations in the magnetization and all explicit magnetostatic effects. For a vicinal surface, dipole-dipole coupling actually induces the spins to lay in the average surface plane of the entire crystal [4] rather than in the plane of the terraces as we have assumed. When combined with crystallographic surface anisotropy, this effect induces a two-fold anisotropy parallel to the steps at all terrace sites.

[21] Such a term is easily included in our basic energy expression (1) and does not appreciably complicate the analysis.

V. SUMMARY

This work was motivated by the increasing awareness that the step structure of ultra-thin magnetic films can have a profound effect on magnetic reversal and hysteresis. Our theoretical study focused on perhaps the simplest case: a film deposited on a vicinal surface comprised of uniform length terraces separated by monoatomic steps. The magnetization was assumed to lay in the plane parallel to the terraces and to vary negligibly in the direction perpendicular to the terraces and parallel to the steps. We assumed the presence of an intrinsic four-fold in-plane anisotropy at every site and a two-fold anisotropy at step sites only. Explicit magnetostatics was ignored. Attention was directed to the interesting case where one orients an external field perpendicular to the direction of the two-fold axes. The final model studied was a one-dimensional, ferromagnetic spin chain in an external field with spatially inhomogeneous anisotropy.

The analysis was performed in the continuum (micromagnetic) limit where the spin configuration is represented by a function $\theta(x)$ that encodes the angular deviation of the magnetization from the external field direction. Four characteristic hysteresis loop topologies were found and designated as “phases” in a two-dimensional diagram labeled by the natural control parameters of the model: a scaled terrace length \mathcal{L} and a scaled step anisotropy strength \mathcal{K} .

The hysteresis loops were characterized by a nucleation field H_N , where the magnetization first deviates from saturation, a step jump field H_S where a jump in magnetization occurs from near saturation to a state where many spins are aligned parallel to the steps, and a terrace field H_T where a jump in magnetization occurs to the nearly reversed state. For large values of \mathcal{L} we found $H_S \sim \exp(-\mathcal{L})$ and $H_T \sim \mathcal{L}^{-\chi}$ with $\chi \simeq 3.7$.

In all cases, reversal initiates at the steps because the torque applied by the local

anisotropy is maximal there in the saturated state. No sharp transition separates the cases of subsequent spin rotation by nearly coherent rotation and subsequent spin rotation by depinning of a 90° domain wall from the steps. It is a crossover phenomenon. The coherent rotation model of Stoner & Wohlfarth (SW) is most appropriate in the lower left corner of our phase diagram. The step depinning picture is most appropriate in the upper right corner of the diagram.

To our knowledge, all existing measurements of the magnetic properties of ultrathin films on vicinal surfaces have been confined to a relatively small portion of our phase diagram. We encourage experiments designed to explore the remaining *terra incognita*.

VI. ACKNOWLEDGMENTS

The authors acknowledge an intellectual debt to Tony Arrott for the the basic premises of this study and they are grateful to Lei-Han Tang for his contribution to our understanding of the single step limit. Ross Hyman was supported by National Science Foundation Grant No. DMR-9531115.

REFERENCES

- [1] U. Gradmann, in *Handbook of Magnetic Materials*, Volume 7, edited by K.H.J. Buschow (Elsevier,1993), Chapter 1.
- [2] B. Heinrich and J.F. Cochran, *Adv. Phys.* **42**, 523 (1993).
- [3] L. Néel, *J. Phys. Radium* **15**, 225 (1954).
- [4] D.S. Chuang, C.A. Ballentine, and R.C. O’Handley, *Phys. Rev. B* **49**, 15084 (1994).
- [5] See the various contributions to *Ultrathin Magnetic Structures*, edited by J.A.C. Bland and B. Heinrich (Springer-Verlag, Berlin, 1994).
- [6] B. Hillebrands, P. Baumgart, and G. Güntherodt, *Phys. Rev. B* **36**, 2450 (1987).
- [7] P. Bruno, G. Bayreuther, P. Beauvillain, C. Chappert, G. Lugert, D. Renard, J.P. Renard, and J. Seiden, *J. Appl. Phys.* **68**, 5759 (1990); M.T. Kief and W.F. Egelhoff, Jr., *J. Appl. Phys.* **73**, 6195 (1993); Y.L. He and G.C. Wang, *J. Appl. Phys.* **76**, 6446 (1994); X. Meng, X. Bian, R. Adbouche, W.B. Muir, J.O. Stöm-Olsen, Z. Altounian, and M. Sutton, *J. Appl. Phys.* **76**, 7084 (1994); F. Baudelet, M.-T. Lin, W. Kuch, K. Meinel, B. Choi, C.M. Schneider, and J. Kirschner, *Phys. Rev. B* **51**, 12563 (1995); M. Giesen-Siebert, F. Schmitz, and H. Ibach, *Surf. Sci.* **336**, 269 (1995).
- [8] A. Moschel, R.A. Hyman, A. Zangwill and M.D. Stiles, *Phys. Rev. Lett.* **77**, 3653 (1996); R.A. Hyman, M.D. Stiles, L.-H. Tang, and A. Zangwill, *J. Appl. Phys.* **81**, 3911 (1997).
- [9] M.E. Buckley, F.O. Schumann, and J.A.C. Bland, *Phys. Rev. B* **52**, 6596 (1995); M.E. Buckley, F.O. Schumann, and J.A.C. Bland, *J. Phys. Cond. Matt.* **8**, L147 (1996).
- [10] M. Kolesik, M.A. Novotny, and P.A. Rikvold, *Phys. Rev. B* **56**, 11791 (1997).
- [11] E.C. Stoner and E.P. Wohlfarth, *Phil. Trans. Roy. Soc.* **A240**, 74 (1948).
- [12] B.N. Filipov, *Phys. Met. Metall.* **22**, No. 3, 22 (1966).

- [13] W.F. Brown, Jr., J. Mag. Mag. Mat. **3**, 295 (1976).
- [14] A.I. Mitsek and S.S. Semyannikov, Sov. Phys. Sol. State **11**, 899 (1969).
- [15] R. Friedberg and D.I. Paul, Phys. Rev. Lett. **34**, 1234 (1975).
- [16] A.S. Arrott and B. Heinrich, J. Mag. Mag. Mat. **93**, 571 (1991); A.S. Arrott, J. Appl. Phys. **69**, 5212 (1991); A.S. Arrott, T.L. Templeton, and Y. Yoshida, IEEE Trans. Mag. **29**, 2622 (1993); A.S. Arrott, in *Nanomagnetism*, edited by A. Hernando (Kluwer, Dordrecht, 1993), pp. 73-85.
- [17] B. Heinrich, S.T. Purcell, J.R. Dutcher, K.B. Urquhart, J.F. Cochran, and A.S. Arrott, Phys. Rev. B **38**, 12879 (1988).
- [18] A. Berger, U. Linke, and H.P. Oepen, Phys. Rev. Lett. **68**, 839 (1992); W. Wulfhekel, S. Knappmann, and H.P. Oepen, J. Mag. Mag. Mat. **163**, 267 (1996).
- [19] J. Chen and J. L. Erskine, Phys. Rev. Lett. **68**, 1212 (1992); J.-S. Suen and J.L. Erskine, Phys. Rev. Lett. **78**, 3567 (1997).
- [20] W. Weber, C. H. Back, and R. Allenspach, Phys. Rev. B **52**, R14400 (1995); W. Weber, C. H. Back, A. Bischof, C. Würsch, and R. Allenspach, Phys. Rev. Lett. **76**, 1940 (1996).
- [21] R.K. Kawakami, E.J. Escoria-Aparicio, and Z.Q. Qiu, Phys. Rev. Lett. **77**, 2570 (1996).
- [22] I.V. Markov, *Crystal Growth for Beginners - Fundamentals of Nucleation, Crystal Growth & Epitaxy* (World Scientific, 1995). The experimental distinction between island growth and step flow growth for Fe/W(110) can be seen easily in the scanning tunneling microscopy results of H.J. Elmers, J. Hauschild, H. Höche, U. Gradmann, H. Bethge, D. Heuer, and U. Köhler, Phys. Rev. Lett. **73**, 898 (1994).
- [23] The case of K_4 favoring orientations rotated by $\pi/4$ is qualitatively different and will be discussed elsewhere.
- [24] Arrott [16] argues persuasively that magnetostatics does not influence the hysteresis

of ultrathin films with in-plane magnetization. The present authors have confirmed this explicitly for a multilayer version of the island model studied in Ref. [8] using the computational methodology of Mansuripur [32].

[25] This is the equation of motion for a kicked rotor in an angle-dependent potential if the variable x is replaced by time. This mechanical analogy can be helpful in much of the qualitative analysis to follow.

[26] See U. Hinzke and U. Nowak, cond-mat/9801154, and H.L. Richards et al., Phys. Rev B **55**, 11521 (1997) for examples of thermally assisted reversal in systems where the reversal is nucleated at edges.

[27] This is clear for all the hysteresis loops depicted in Figure 3 where H_T is labeled except Phase III. There, there is an inner loop (not shown) that passes through $M = 0$ at $H = 0$.

[28] R.P. Coburn, S.J. Gray and J.A.C. Bland, Phys. Rev. Lett. **79**, 4018 (1997) and references therein.

[29] P. Bak, Rep. Prog. Phys. **45**, 587 (1982).

[30] Our formulae (13) and (16) should be modified to reflect the actual anisotropies assumed in Ref. [21]. Our point is that a pure Stoner-Wohlfarth type analysis will be sufficient.

[31] G.S. Bales and A. Zangwill, Phys. Rev. B **41**, 5500 (1990).

[32] M. Mansuripur, *The Physical Principles of Magneto-optical Recording* (Cambridge University Press, Cambridge, 1995), Section 13.2.

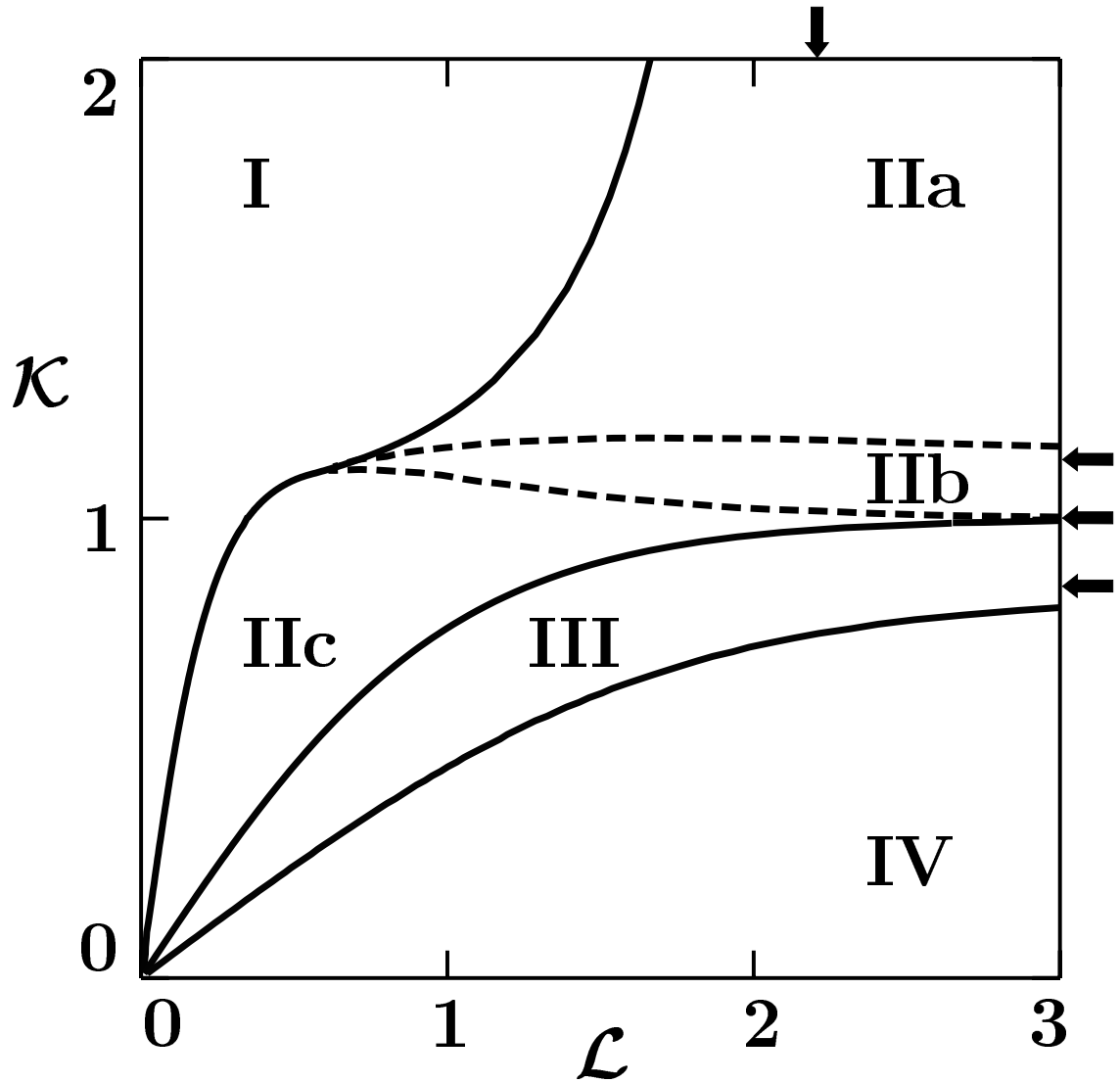


FIG. 2. Loop structure phase diagram. The independent variables are a scaled two-fold anisotropy strength at the step, \mathcal{K} and a scaled step separation \mathcal{L} . Roman numerals label four distinct loop topologies. Lower case letters label three variants of Phase II. The vertical and horizontal arrows respectively show the $\mathcal{K} \rightarrow \infty$ and $\mathcal{L} \rightarrow \infty$ limits of the nearby phase boundaries.

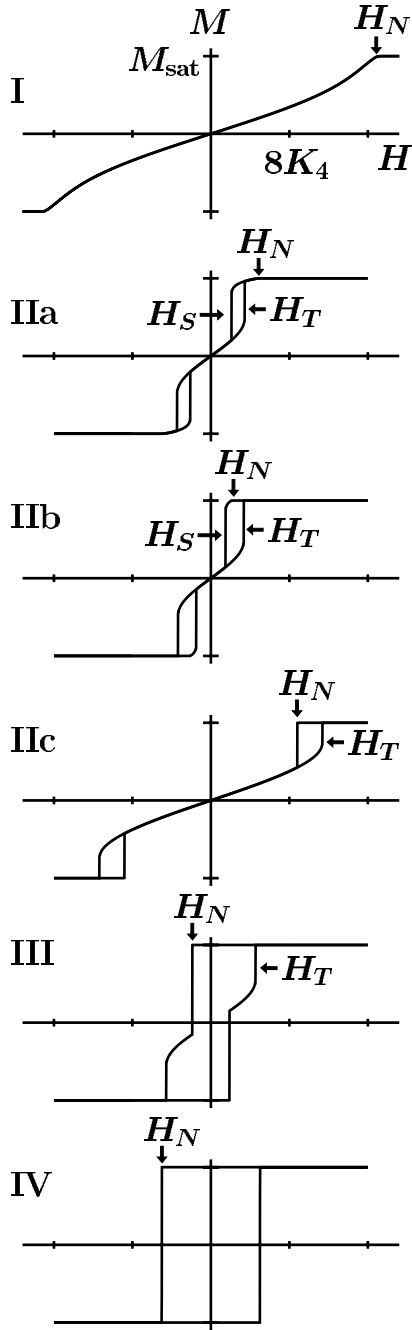


FIG. 3. Hysteresis loops. The type of hysteresis loop in different parts of the phase diagram, (see Fig. 2). The scaled parameters for each loop are: I, $\mathcal{K} = 1.25$, $\mathcal{L} = 0.5$; IIa, $\mathcal{K} = 1.25$, $\mathcal{L} = 2.0$; IIb, $\mathcal{K} = 1.1$, $\mathcal{L} = 2.0$; IIc, $\mathcal{K} = 0.5$, $\mathcal{L} = 0.25$; III, $\mathcal{K} = 0.5$, $\mathcal{L} = 0.75$; IV, $\mathcal{K} = 0.5$, $\mathcal{L} = 2.0$.

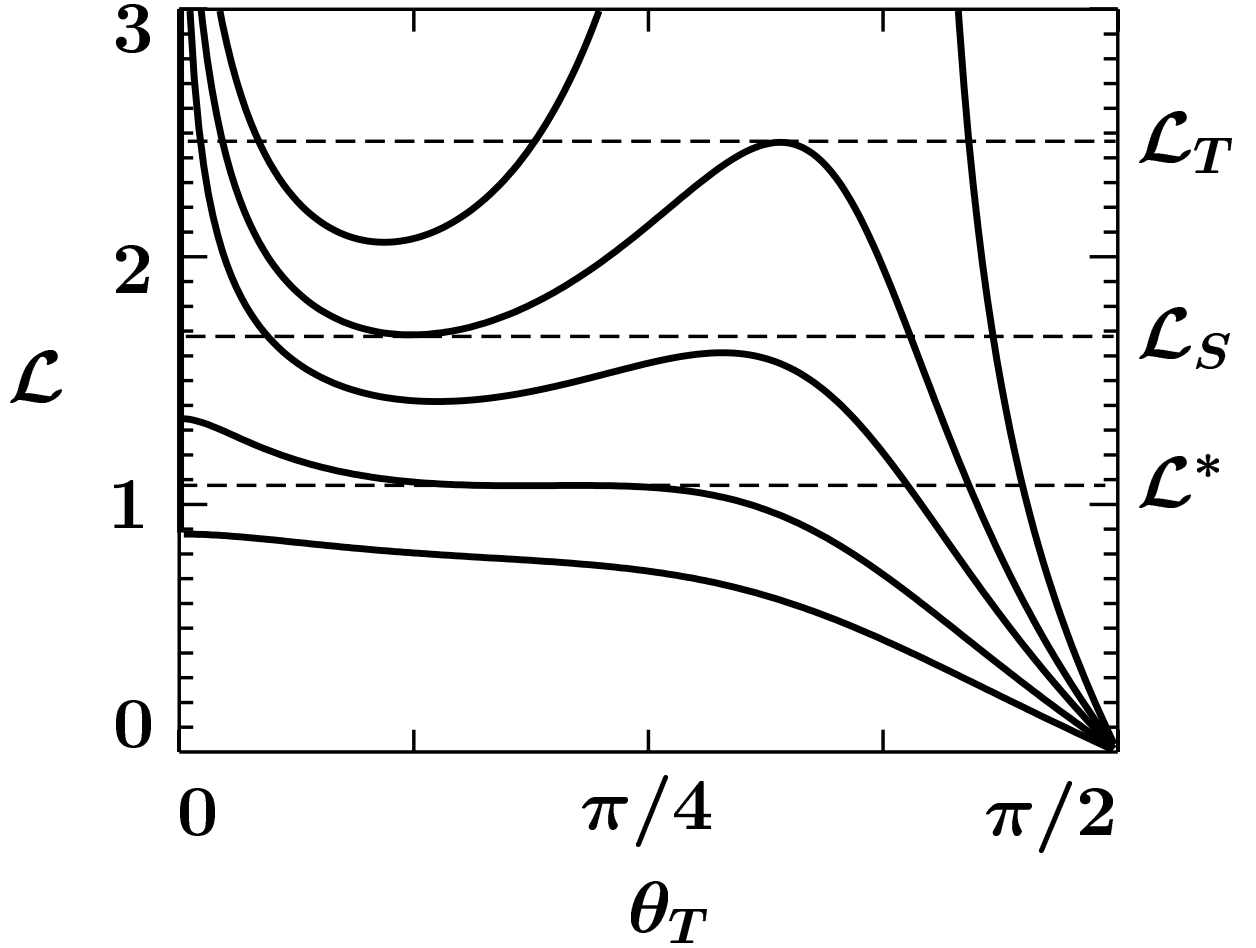


FIG. 4. Scaled terrace width \mathcal{L} as a function of terrace spin angle θ_T for $\mathcal{K}= 1.25$ and $\mathcal{H}= 2, 3, 4, 6, 9$. The value of \mathcal{H} decreases monotonically as the sequence of curves is traversed from bottom to top. The horizontal dashed lines labeled \mathcal{L}^* , \mathcal{L}_S , and \mathcal{L}_T are discussed in the text.

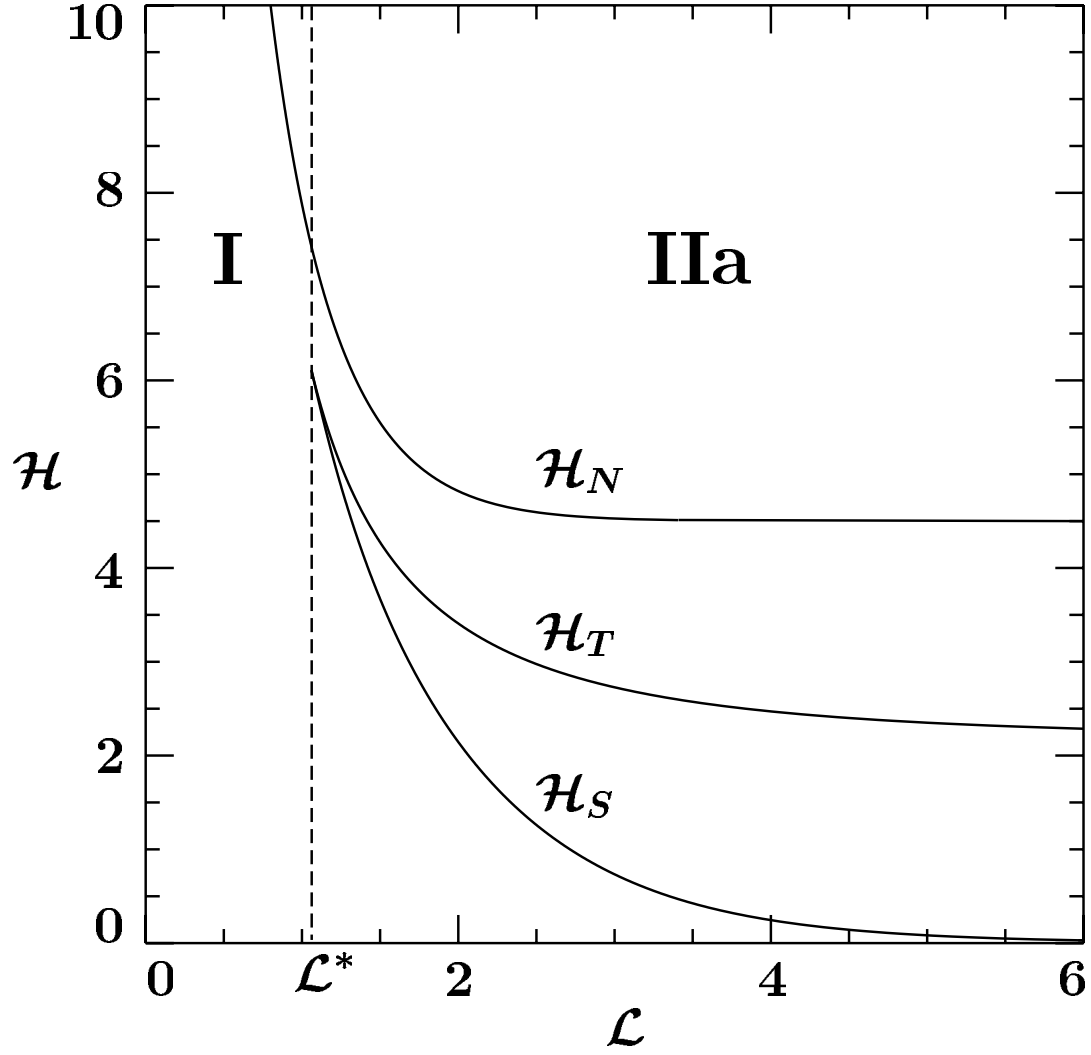


FIG. 5. Characteristic fields for $\mathcal{K} = 1.25$. The vertical dashed line $\mathcal{L} = \mathcal{L}^*$ is the I-IIa phase boundary. See text for discussion.

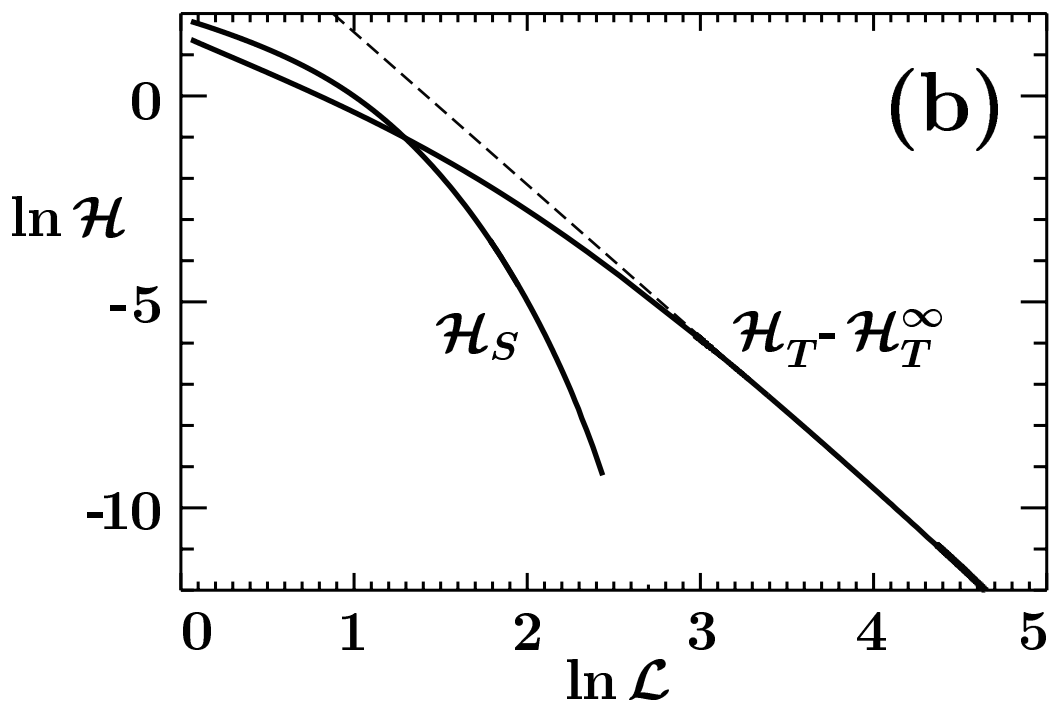
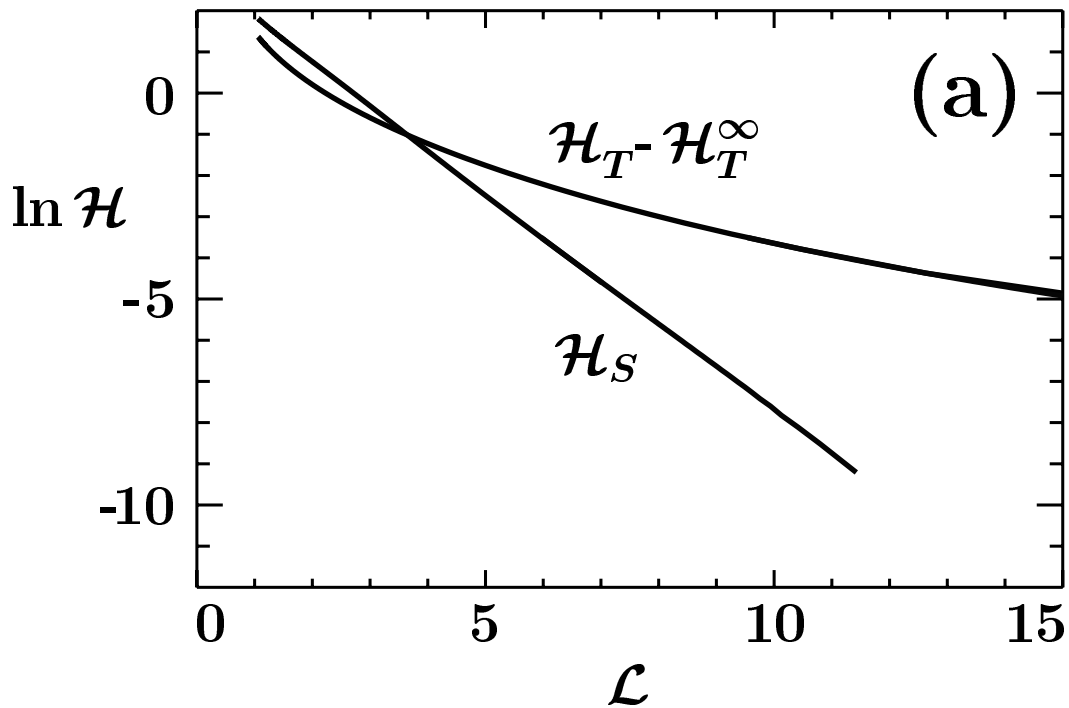


FIG. 6. Asymptotic behavior of the fields \mathcal{H}_S and $\mathcal{H}_T - \mathcal{H}_T^\infty$ for large \mathcal{L} . Note that $H_S^\infty = 0$.(a) Log-linear plot. (b) Log-Log plot. Straight line has a slope of -3.7

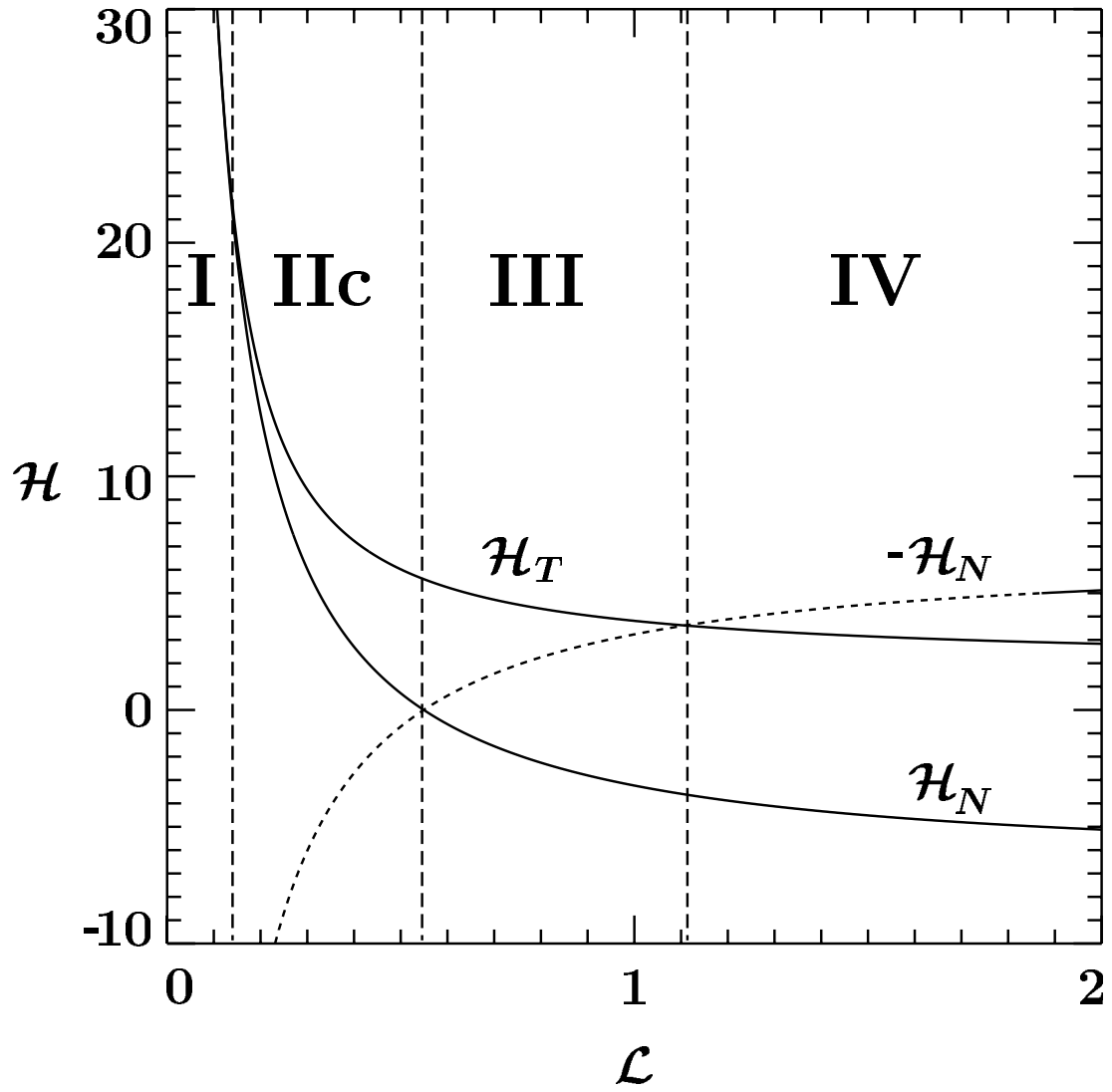


FIG. 7. Characteristic fields for $\mathcal{K} = 0.5$. Vertical dashed lines denote phase boundaries. See text for discussion.

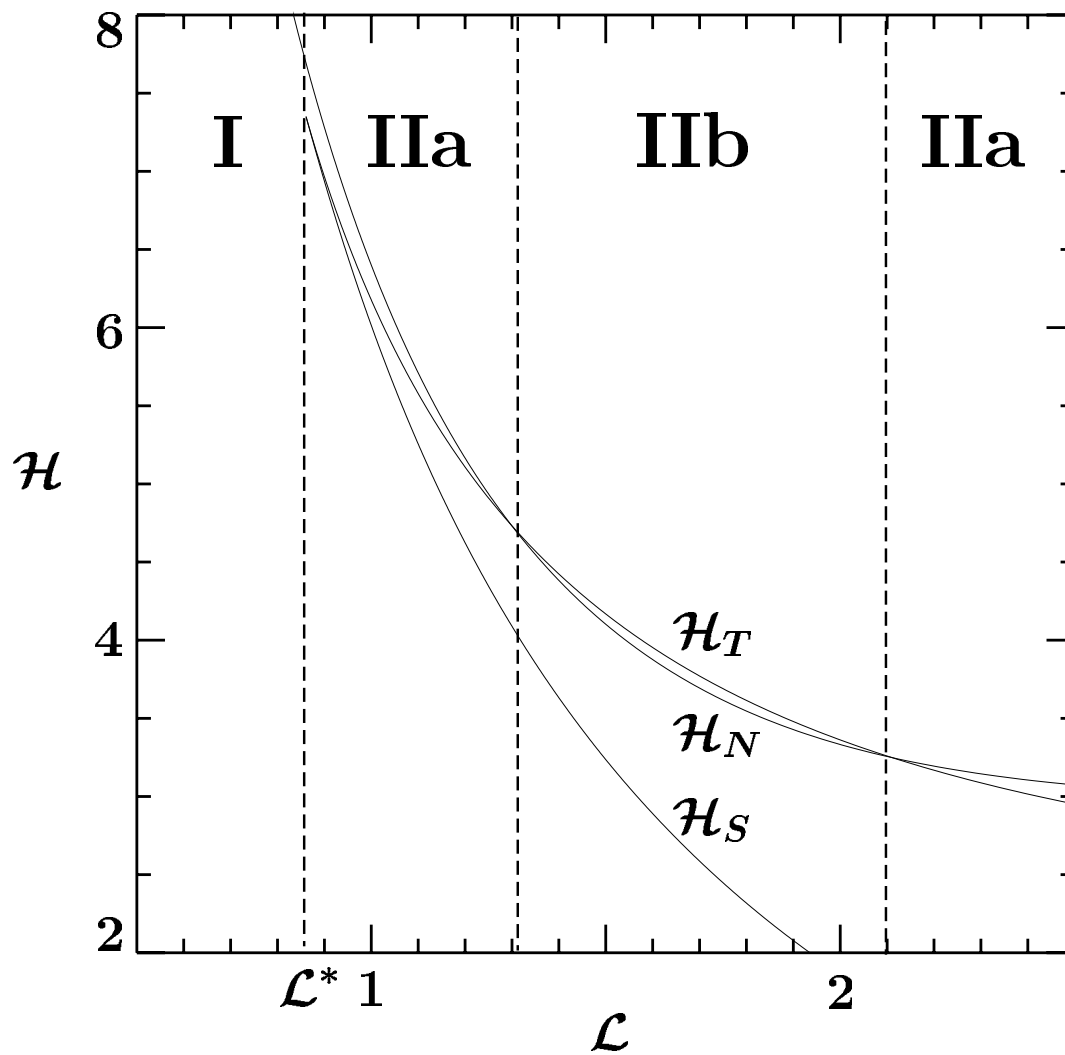


FIG. 8. Characteristic fields for $\mathcal{K} = 1.17$. Vertical dashed lines denote phase boundaries. See text for discussion.